ORNL/SR-2017/346

RIA simulation tests using driver tube for ATF cladding

Nuclear Technology Research and Development

Approved for Public Release.

Prepared for
U.S. Department of Energy
Advanced Fuel Campaign
M. N. Cinbiz
N. R. Brown
R. R. Lowden
K. Linton
K. A. Terrani
Oak Ridge National Laboratory
July 2017
M3FT-17OR020204032

SUMMARY

Pellet-cladding mechanical interaction (PCMI) is a potential failure mechanism for accident-tolerant fuel (ATF) cladding candidates during a reactivity-initiated accident (RIA). This report summarizes Fiscal Year (FY) 2017 research activities that were undertaken to evaluate the PCMI-like hoop-strain-driven mechanical response of ATF cladding candidates. To achieve various RIA-like conditions, a modified-burst test (MBT) device was developed to produce different mechanical pulses. The calibration of the MBT instrument was accomplished by performing mechanical tests on unirradiated Generation-I iron-chromium-aluminum (FeCrAl) alloy samples. Shakedown tests were also conducted in both FY 2016 and FY 2017 using unirradiated hydrided ZIRLO™ tube samples. This milestone report focuses on testing of ATF materials, but the benchmark tests with hydrided ZIRLO™ tube samples are documented in a recent journal article.[a] For the calibration and benchmark tests, the hoop strain was monitored using strain gauges attached to the sample surface in the hoop direction.

A novel digital image correlation (DIC) system composed of a single high-speed camera and an array of six mirrors was developed for the MBT instrument to better resolve the failure behavior of samples and to provide useful data for validation of high-fidelity modeling and simulation tools. The DIC system enable a 360° view of a sample's outer surface. This feature was added to the instrument to determine the precise failure location on a sample's surface for strain predictions. The DIC system was tested on several silicon carbide fiber/silicon carbide matrix (SiC/SiC) composite tube samples at various pressurization rates of the driver tube (which correspond to the strain rates for the samples). The hoop strains for various loading conditions were determined for the SiC/SiC composite tube samples.

Future work is planned to enhance understanding of the failure behavior of the ATF cladding candidates of age-hardened FeCrAl alloys and SiC/SiC composites in detail during RIA conditions informed by the computational studies performed under the US Department of Energy Office of Nuclear Energy Advanced Fuels Campaign. The testing instrument and the new DIC system will be further developed to reach different stress-state conditions and to perform tests at elevated temperatures.

[a] Cinbiz, M. N., N. R. Brown, K. A. Terrani, R. R. Lowden, and D. Erdman, (2017). A pulse-controlled modified-burst test instrument for accident-tolerant fuel cladding. *Annals of Nuclear Energy* 109, 396–404.

INTENTIONALLY BLANK

CONTENTS

FIGURES

TABLES

ACRONYMS

AFC	Advanced Fuels Campaign
ATF	accident tolerant fuel
ATR	advanced test reactor
ATWS	anticipated transient without SCRAM
BWR	boiling water reactor
DBA	design basis accident
DOE	US Department of Energy
EPRI	Electric Power Research Institute
FeCrAl	iron-chromium-aluminum alloy
INL	Idaho National Laboratory
LOCA	loss-of-coolant accident
LWR	light water reactor
MBT	modified-burst test
NRC	US Nuclear Regulatory Commission
NSRR	Nuclear Safety Research Reactor
ORNL	Oak Ridge National Laboratory
PCMI	pellet cladding mechanical interaction
PWR	pressurized water reactor
RIA	reactivity initiated accident
SiC	silicon carbide
SiC/SiC	silicon carbide fiber silicon carbide matrix
TREAT	Transient Reactor Test Facility

ACKNOWLEDGMENTS

This work was supported by the US Department of Energy Office of Nuclear Energy (DOE-NE) Advanced Fuels Campaign (AFC). The authors thank Daniel M. Wachs of Idaho National Laboratory for his oversight of this area.

RIA SIMULATION TESTS USING DRIVER TUBE FOR ATF CLADDING

1. INTRODUCTION

The US Department of Energy Office of Nuclear Energy Advanced Fuels Campaign is working closely with the nuclear industry, national laboratories, and academia to develop light water reactor (LWR) fuel and core materials with potentially enhanced accident tolerance, also known as "accident-tolerant fuel" (ATF) [1]. The technical objective of developing candidate ATF materials is to enhance nuclear fuel and cladding performance during beyond-design-basis accidents by increasing the amount of coping time without active core cooling during a severe accident [2]. To directly address the beyond-design-basis accident at the Fukushima Daiichi Nuclear Power Station in 2011, enhanced accident tolerance should be achieved by improving high-temperature steam oxidation resistance [2–4]. ATF fuel and cladding materials must also at least maintain the reactor performance and safety characteristics of the present uranium dioxide and zirconium-based alloy fuel systems during normal operation, operational transients, and postulated design-basis accidents such as a loss of coolant accident (LOCA) or a reactivity-initiated accident (RIA) [5]. LOCA behavior is anticipated to improve with the introduction of the candidate ATF cladding materials because of their high mechanical strength at elevated temperatures (from 800°C to 1,000°C) in a steam environment. However, the mechanical response of the candidate ATF cladding alloys has not been determined under conditions that emulate those caused by pellet-cladding mechanical interaction (PCMI) due to rapid thermal expansion of the fuel during an RIA.

A control rod ejection accident and a control rod drop accident are forms of RIAs that could occur in a pressurized water reactor (PWR) or a boiling water reactor (BWR), respectively. During a control rod ejection or control rod drop, positive reactivity is inserted as result of removal of the control rods from the core. This leads to an exponential increase in the fission rate until the power pulse is turned around by fuel temperature feedback. The nearly adiabatic energy deposition during the event causes a rapid temperature increase in the fuel pellets, which results in rapid thermal expansion of the fuel. If the fuel-cladding gap has closed prior to, or closes during, the RIA, the expansion of the fuel may cause a PCMI. The PCMI will impose a biaxial strain state on the cladding [6]. The power pulse occurs on a time scale of tens of milliseconds and may cause cladding failure if the cladding is overstrained.

The following requirements are found in the General Design Criteria [7]:

The reactivity control systems shall be designed with appropriate limits on the potential amount and rate of reactivity increase to assure that the effects of postulated reactivity accidents can neither (1) result in damage to the reactor coolant pressure boundary greater than limited local yielding nor (2) sufficiently disturb the core, its support structures or other reactor pressure vessel internals to impair significantly the capability to cool the core. These postulated reactivity accidents shall include consideration of rod ejection (unless prevented by positive means), rod dropout, steam line rupture, changes in reactor coolant temperature and pressure, and cold water addition.

The mechanical viability of ATF cladding must be studied to determine the applicable failure limits of the cladding [8,9]. Separate-effects, and later integral-effects, tests must be conducted on candidate ATF cladding materials to determine appropriate safety limits and failure mechanisms.

A variety of in-pile tests relevant to the PCMI phase of RIAs have been conducted at transient test reactors. Most in-pile tests have been conducted at reactors that do not have reactor kinetics parameters directly relevant to PWRs or BWRs [e.g., the Nuclear Safety Research Reactor (NSRR) in Japan]. The pulse width of a super-prompt RIA is a direct function of the following parameters: (1) inserted reactivity, (2) prompt temperature feedback coefficients, (3) volumetric heat capacity, and (4) neutron generation time. Some examples of different pulse characteristics from transient test reactors are shown in Figure 1,

including the Transient Reactor Test Facility (TREAT) at Idaho National Laboratory (INL), the CABRI reactor at Cadarache in France, the Power Burst Facility (PBF) at INL (defueled, to be demolished), and the NSRR. A large degree of variation in the pulse width and the strain rate is expected in various transient test reactors because the temperature increase rate in a fuel pellet and its associated thermal expansion rate are proportional to the pulse. The long-term goal for the pulse-controlled modified-burst test (MBT) is that it will act as a separate-effects test that bridges the gap between the various in-pile tests because it is capable of simulating mechanical pulses between 10 and 100 ms.

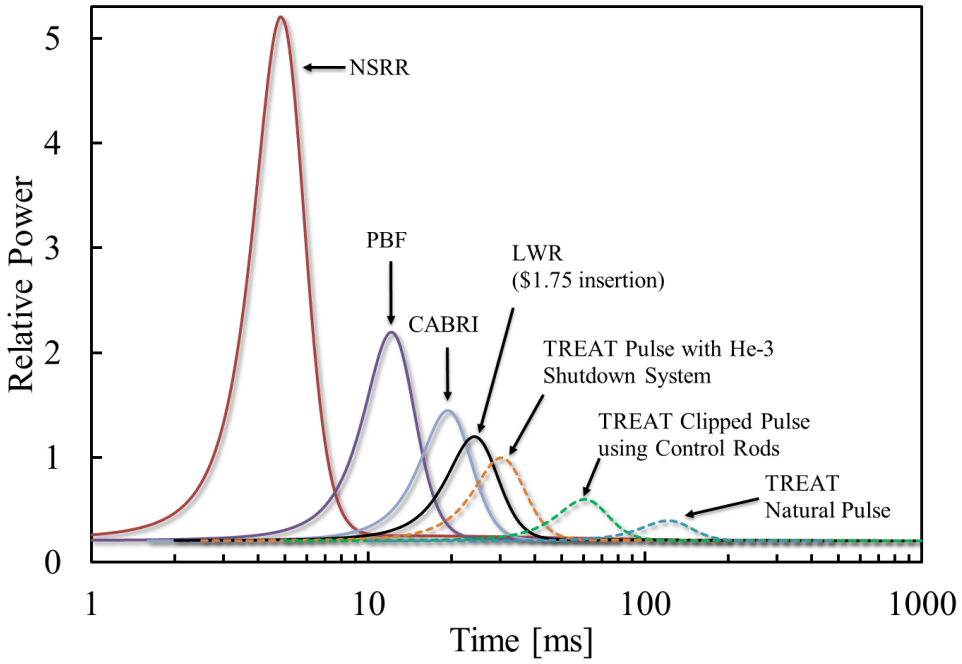

Figure 1 Representative pulses from various in-pile transient test reactors and a generic light water reactor, assuming a constant energy deposition. $1.75 insertion refers to the positive reactivity insertion during a RIA transient.

Separate-effects tests inform the design of integral-effects tests to investigate the transient response of the ATF fuel rods during RIA-relevant conditions. To support the design of future in-pile integral experiments and to capture distinct reactor kinetics of distinct reactors (see Figure 1), the separate-effects test is a vital tool that can be used to replicate the time scale of an RIA event by mimicking the mechanical loading conditions as a result of the energy input during the RIA.

The MBT achieves straining conditions at strain rates of an anticipated RIA in a typical LWR. The MBT is an indirect mechanical test, similar to the mandrel-driven and the plug-expansion tests. The mechanical straining of samples is caused by the motion of another object located inside a tube sample, such as a driver tube for MBT [10,11], ceramic pieces for a mandrel-driven test [12,13] and a polymer pellet for plug-expansion test [14–16]. For an MBT, the deformation of the sample is initiated by the pressurization of an another closed-end tube, which is made of an age-hardened Inconel alloy. Only mechanical strain is monitored during mechanical testing due to the indirect loading, which is similar to that hypothesized during a PCMI loading. Because the mechanical failure of cladding is driven by cracks or voids initiated by hoop strain, the data produced by the tests inform development and validation of micromechanical failure models.

In this report, we have improved the MBT instrument (designed in FY 2016) by making it capable of simulating various mechanical pulses. The strain data can be acquired using either strain gauges or a novel digital image correlation (DIC) system with a mirror arrangement that captures a 360° view the outer

surface of a sample tube. The control of the mechanical pulse was tested by performing experiments on Generation-I (Gen-I) iron-chromium-aluminum (FeCrAl) alloys using a strain gauge attached to the sample surface. [The alloys referred to as "Gen-I" possess a nonoptimal large grain size (80–100 μm)] The novel DIC system was tested by conducting SiC/SiC composite experiments at various pressurization rates.

2. CONTROL OF THE MECHANICAL PULSE OF MBT INSTRUMENT

This section describes the test device and its calibration results using FeCrAl samples. To provide a review of the MBT instrument operation, sections 2.1 and 2.2 are reproduced directly from References 15 and 16.

2.1 Control of the Internal Pressure of the Driver Tube

The working principles of the MBT are described in a report from FY 2016 [17] and in several references in the open literature [10,11]. The driver tube is pressurized by the motion of a core pin, which is initiated by a strike pin, where the displacement and speed of the strike pin are independently controlled by a hydraulic actuator [17]. Therefore, the rate and amplitude of the internal pressure of the driver tube can be finely tuned by manipulation of the core-pin displacement and speed through the driver tube (see Figure 2). The objectives of this fine control are to elucidate any impact of the strain rate on the failure of the cladding and to be capable of simulating RIA scenarios over a range of pulse widths, including the pulse shapes of the in-pile experiments shown in Figure 1. The parameters that dictate the motion of the core-pin into the driver tube are the displacement (d_1) and the speed of the core pin (Figure 2), both of which were controlled using a hydraulic press with precise displacement control.

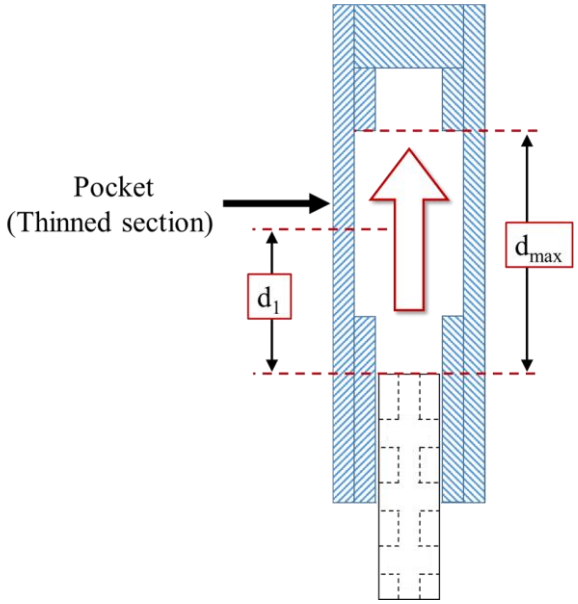

Figure 2 Schematic of the axial cross section of the driver tube, highlighting the core-pin displacement (d_1).The maximum allowed displacement of core-pin in the driver tube is d_{max}

The effect of core-pin displacement and core-pin speed on the internal pressure of the driver tube is shown in Figure 3. Figure 3(a) shows the internal pressure of the driver tube during a series of tests while

core-pin displacement was varied at a constant core-pin speed. The core-pin displacement in the driver tube was increased at the same velocity (1.016 m/s) from 0.01016 to 0.01540 m, but the internal pressure increased from 56 to 232 MPa. The pressurization rates for each of the displacement cases were determined to be 6.4 GPa/s for 0.01016 m, 13.4 GPa/s for 0.01270 m, and 19.8 GPa/s for 0.01540 m. Figure 3(b) emphasizes the effect of the core-pin velocity at constant core-pin displacement. When core-pin speed was varied from 0.254 to 1.016 m/s at a same core-pin displacement (0.0127 m), the driver tube pressure rise time was reduced from 32.2 to 13 ms. All the tests reached similar internal pressures: 157 MPa at 0.0127 m/s, 162 MPa at 0.508 m/s, and 166 MPa at 1.016 m/s.

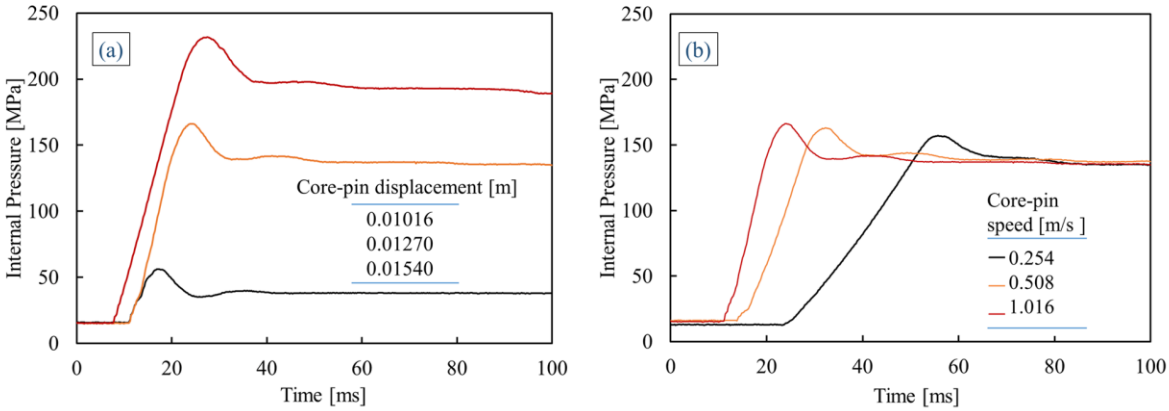

Figure 3 The effect of (a) core-pin displacement and (b) core-pin speed on the internal pressure of the driver tube.

2.2 Calibration of the Pulse-controlled MBT Instrument using FeCrAl

Unirradiated Gen-I FeCrAl tube cladding specimens were subjected to calibration tests to determine their transient mechanical responses with emphasis on transient-event occurrence time, similar to in-pile testing of reactor transients [8,18–21]. The Gen-I FeCrAl samples had an outer diameter of 8.63 mm, a wall thickness of 0.44 mm, and a nonoptimal large grain size (80–100 μm). (Figure 4). The samples were without solid solution strengthening or precipitation hardening [22].

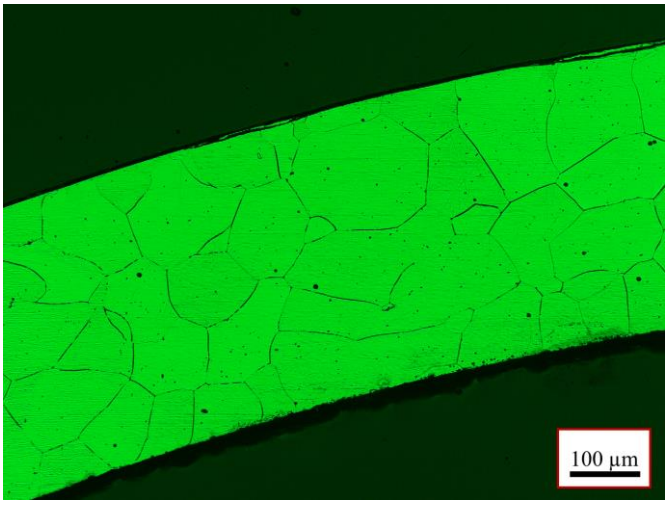

Figure 4. Microstructure of Gen-I FeCrAl alloy utilized in this study.

In the tests, FeCrAl samples were not strained to rupture due to their high ductility [23], and samples were kept in the elastic region to investigate the mechanical response of FeCrAl. Figure 5 shows the response of the FeCrAl samples at various core-pin speeds and at similar pressurization amplitudes. As the core-pin speed was increased from 0.0254 to 0.508m/s, the pressurization time decreased from 266 to 13.01 ms. For core-pin speeds of 0.127 and 0.254 m/s, pressure rise times were 32.4 and 55.8 ms. Time differences between strain and pressure rise times were relatively small, approximately 2.5, 1.8, 4.6, and 7.9 ms for core-pin velocities of 0.0254, 0.127, 0.254, and 0.508 m/s, respectively. The scoping tests indicate that, by using parameters to control core-pin speed, a variety of transient mechanical loading conditions can be imposed on ATF cladding to investigate RIA-like behavior. Thus the conditions similar to the in-pile integral effects (see Figure 1) can be replicated by ex situ separate-effects tests to develop failure models.

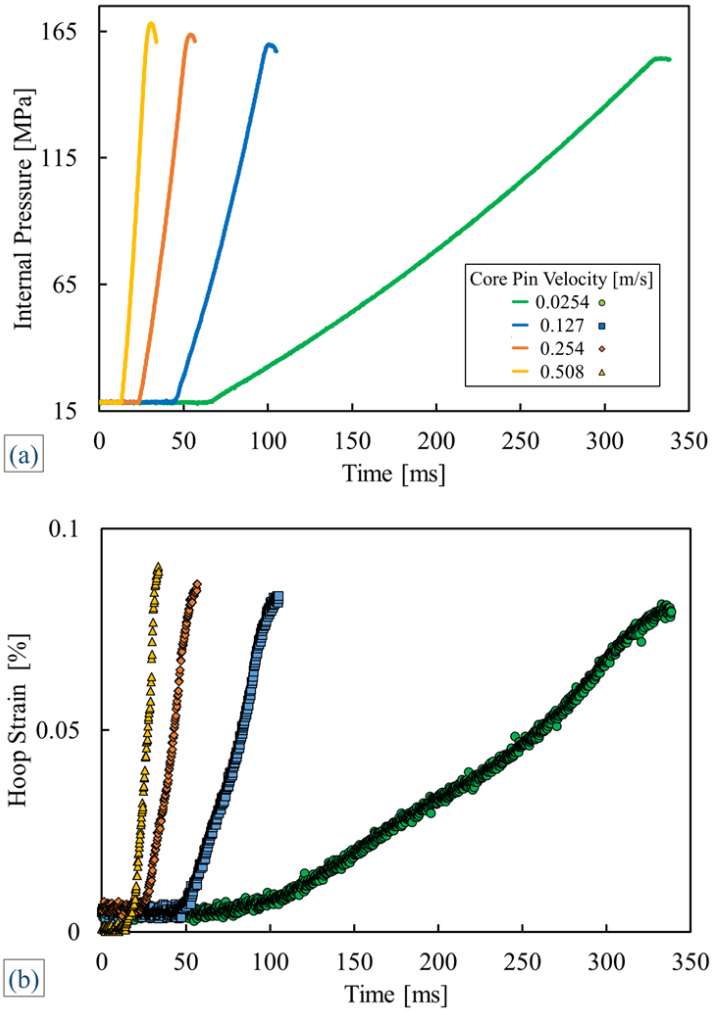

Figure 5 Mechanical pulse shapes for model Gen-I FeCrAl alloys. Driver tube internal pressure (b) hoop strain. No cladding rupture/failure occurred.

3. DIC SYSTEM AND A MIRROR ARRANGEMENT FOR 360°-VIEW OF SAMPLES

The failure location of a tube specimen that is subjected to a MBT is known to some extent in the axial direction because of the internal geometry of the driver tube, which has a thinned pocket that is 0.25 or 0.5 in. long (see Figure 2). The failure location in the hoop direction of the sample can be anywhere in that pocket and thus affects the determination of the sample failure strain. The strain gauges attached to the samples may not monitor the failure hoop strain because the rupture location may not be at the place where the strain gauge is located. Therefore, utilization of a strain gauge does not necessarily guarantee that the hoop strain measurement will be representative of the failure strain of the sample. Rather, the strain gauge reading represents the local strain at the point where it attached to the sample surface. Furthermore, a DIC-aided strain measurement that is acquiring data from only one surface cannot capture the failure location unless the failure location is on the monitored surface of the sample.

A specialized DIC system was developed to resolve these challenges and to offer a high-resolution depiction of sample failure. Determining the exact location of failure for tube samples requires a 360° view of the outer surface of the tube sample. To achieve such observations, a DIC system with multiple cameras or one camera with an appropriate mirror arrangement is required. In this study, we developed a DIC system with a mirror setup that enables a 360° view of the sample surface (see Figure 6). Because an MBT-induced failure occurs in 10 to 300 ms, the DIC system also uses a high-speed camera that is capable of recording sample deformation during testing.

The 360° view of a sample's reflection is acquired by one camera (Photron AX-200), one telecentric lens (Opto Engineering TC16M 120), and six first-surface mirrors as depicted in the schematics (Figure 6). Telecentric lenses are utilized for the elimination of the tube expansion effect on the strain calculations. The 360° view of the sample is obtained from the sample reflections on the mirrors.

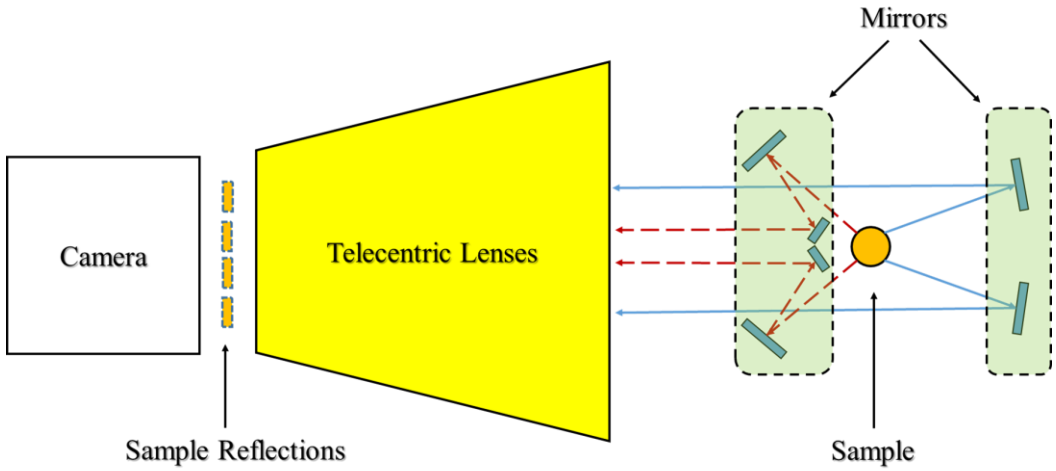

Figure 6 Schematics of the digital image correlation setup with a single camera and an arrangement of multiple mirrors.

4. PCMI TESTING OF SiC/SiC AT RIA-LIKE CONDITIONS

This section describes the mechanical behavior of triaxially braided SiC/SiC composite tube samples subjected to MBT to simulate PCMI loading conditions at RIA-relevant strain rates. Driver tubes were subjected to various pressurization rates that generate distinct straining conditions for SiC/SiC samples. The single-camera DIC system was used to gather data during the testing. AsphyreDIC, a custom-built DIC software, was used to determine the failure hoop strain from the acquired data.

4.1 Materials and Experimental Parameters

The SiC/SiC composite samples are the General Atomics triaxially braided SiC/SiC architecture of Hi Nicalon^{TM} type S fibers with pyrolytic carbon (PyC) interphase for cladding tube applications. The PyC interphase was initially deposited via chemical vapor deposition on the preform SiC fibers. Fiber bundles were oriented 0° and ± 45° with the tube axial direction as shown in Figure 7. The SiC/SiC composite was fabricated by chemical vapor infiltration. The initial porosity of fibers was 10%.

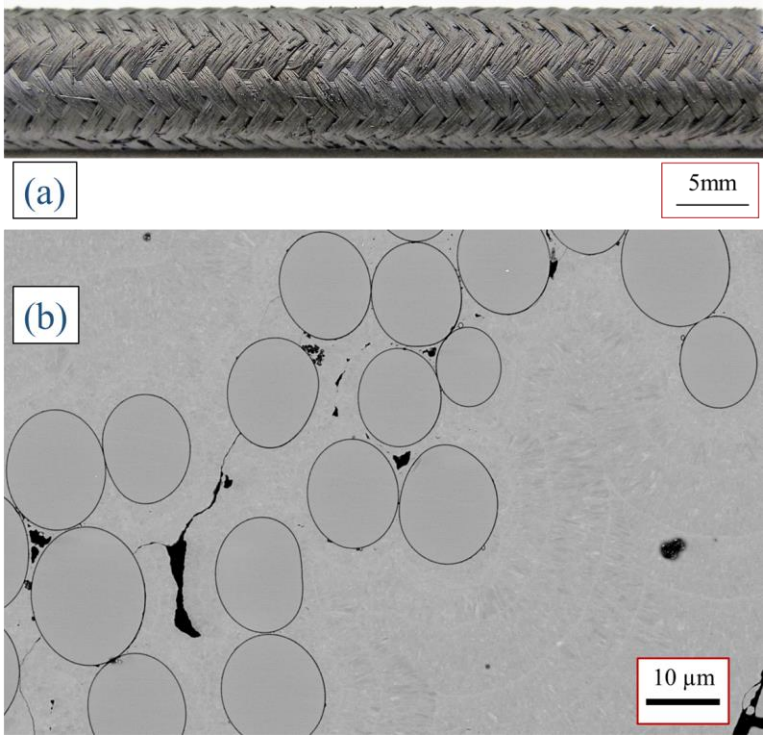

Figure 7 (a) Triaxially-braided SiC/SiC tube (b) fiber microstructure of the SiC/SiC.

Table 1 shows the experiment matrix and loading conditions for the SiC/SiC composites. Samples were subject to mechanical loading up to rupture at three different event-occurrence times. The testing parameters were generated by controlling the core-pin speed (10, 30, and 50 in./s) and core-pin displacement (0.8 in.) using two driver tube geometries with pocket sizes of 0.5 and 0.25 in. The effect of the pocket size was investigated by conducting experiments at a core-pin speed of 50 in./s. Three samples were tested using a 0.5 in. driver tube to investigate the pressurization rate of the driver tube, which corresponds to the strain rate on the sample,

Speckle patterns of white and black dyes were applied to the sample surface. DIC data was gathered at a rate from 6400 to 12500 Hz at resolutions of 1024 × 1024 and 1024 × 672 pixels from four sides of each sample. The acquired speckle images of the reflected surfaces of the samples were analyzed using custom-prepared analysis software.

Table 1. The proposed experiments and core-pin parameters of the modified-burst test. Core-pin displacement of 0.8 in. ensured the failure of the SiC-SiC composite samples

Experiment number	Sample identification	Driver tube thin-section size (in.)	Core-pin speed (in./s)	Core-pin displacement (in.)	Frame rate (fps)	Resolution (pixel × pixel)
1	SiC-1B	0.5	10	0.8	6400	1024 × 1024
2	SiC-3B	0.5	30	0.8	10000	1024 × 672
3	SiC-5B	0.5	50	0.8	12500	1024 × 672
4	SiC-4B	0.25	50	0.8	12500	1024 × 672

4.2 Preliminary SiC/SiC Results and Analysis

This report focuses on the DIC analysis results of one sample (SiC-5B), which is subject to core-pin speed of 50 in./s and core-pin displacement of 0.5 in. These preliminary data are shown to depict typical mechanical data obtained from the developed DIC system. Figure 8 shows sequential pictures of the 360° view of the sample's outer surface at the moment just before failure, where sample integrity was still maintained [Figure 8(a)], at the outer fiber rupture [Figure 8 (b)], and at the final rupture [Figure 8 (c)]. Figure 8 (b) captured the moment of the rupture of the outer surface fibers before ultimate failure. Furthermore, DIC objects utilized to perform DIC analysis were shown on the sample surface at the failure location. To ensure that the sample was completely in focus, the failure strain was estimated using the image frame just before the rupture was recorded.

Figure 9 shows evolution of the internal pressure of the driver tube and the DIC-calculated hoop and axial strains on the SiC/SiC composite sample (SiC-5B). The internal pressure in the driver tube increased to 209 MPa within 19.3 ms and led to the sample failure at hoop and axial strains of 0.48%. The strain value was determined by the point object shown in Figure 8 (b). Each strain data point represents an image taken by camera at resolution of 1024 × 670 and at 12500 Hz. As internal pressure started to increase at t=6.2 ms, the hoop strain increased and axial strain started to decrease. However, the axial strain started to increase at t=25 ms. The increase in axial strain persisted until sample failed at 26.9 ms. DIC analysis of the strain values on the point object shown in Figure 8 (c) indicates that the strain biaxiality ratio ($\varepsilon_2/\varepsilon_1$) reached a nearly equibiaxial strain state at rupture, as depicted in Figure 9.

Evolution of the internal pressure and the DIC calculated strain data were also gathered for other samples listed in Table 1. For convenience, only one sample's DIC results were shown in this report. The failure hoop strains of all samples and the pressurization rates of the driver tubes are reported in Table 2. Sample SiC-1B, which was pressurized at a low rate (3 GPa/s), ruptured at the failure strain of 0.25% and at internal pressure of 170 MPa, whereas samples subjected to high pressurization rates (~8 GPa/s) failed at higher hoop strains, as shown in Table 2. Furthermore, the internal pressure of the driver tubes of these samples were all above 200 MPa.

.

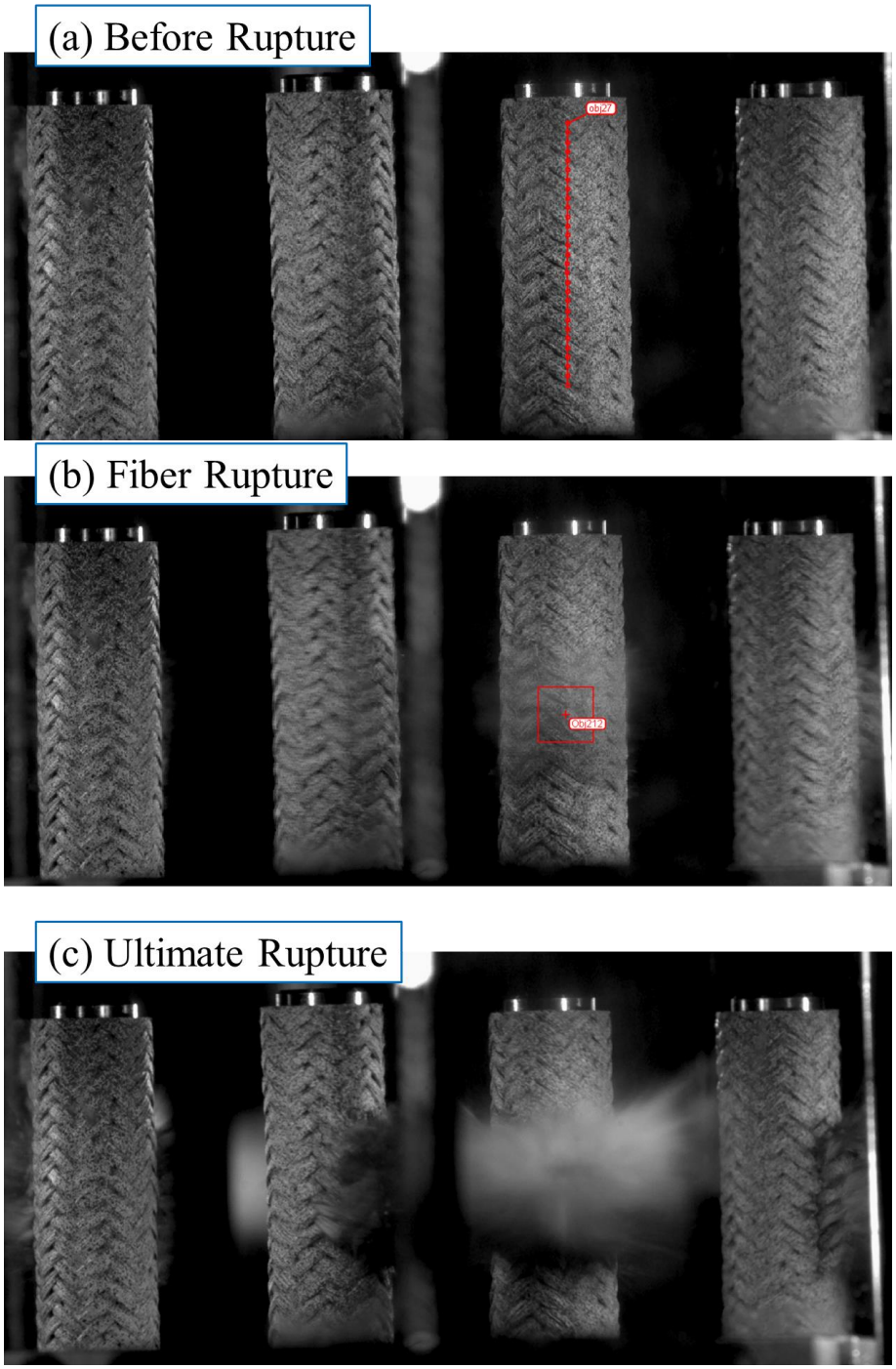

Figure 8 360° view of the outer surface of the SiC/SiC composite sample before fracture (a), at the fiber rupture (b), and at the ultimate fracture (c).

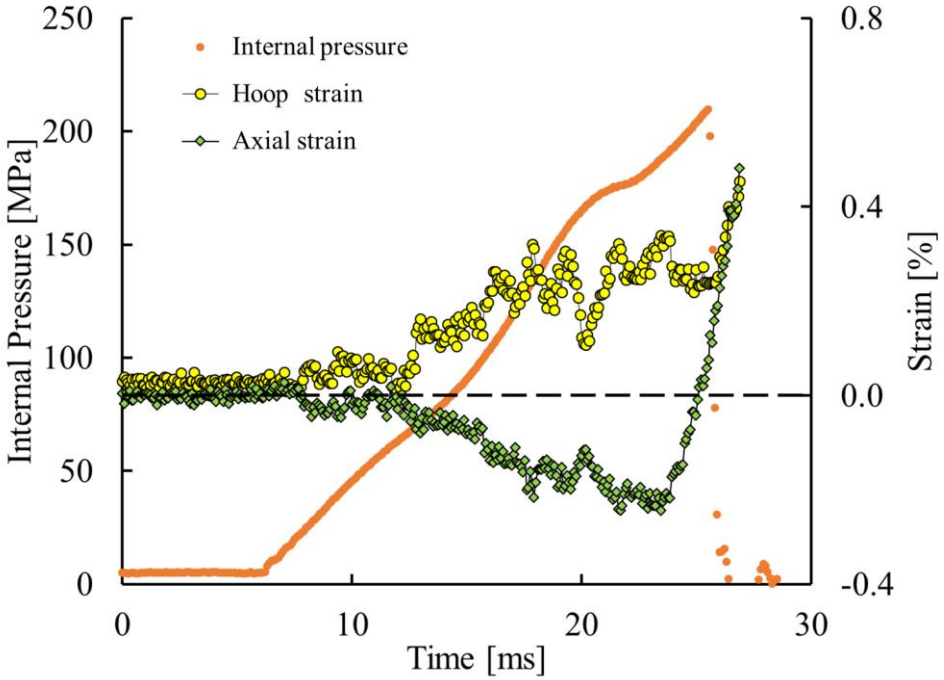

Figure 9 Evolution of internal pressure of the driver tube and the DIC-calculated hoop and axial strains on the SiC/SiC composite.

Figure 10 shows the hoop and axial strain distributions along the line shown in Figure 8a before rupture. The hoop strain on the SiC/SiC increased at the thinned-region of the driver tube up to the value of 0.6% which was estimated to be the failure strain. The axial strain was increased to 0.25% at the same location. The strain biaxiality ratio at the failure location was calculated as 0.42. Axial strain was also negative on sample locations which correspond to the boundaries of the pocket, indicating a sample contraction along the axial direction of sample. A complex state of strain was indicated on the sample surface subjected to the MBT.

Table 2 The internal pressure and failure strains of th SiC/SiC samples. Failure strain is determined using point objects on the captured image before rupture.

Sample Identification	Internal Pressure at Rupture [MPa]	Pressurization Rate [GPa/s]	Strain at Failure [%]	Frame Rate [fps]
SiC-1B	170	3	0.25	6400
SiC-3B	249	8.7	0.45	10000
SiC-5B	209	8.1	0.85	12500
SiC-4B	238	8.8	0.82	12500

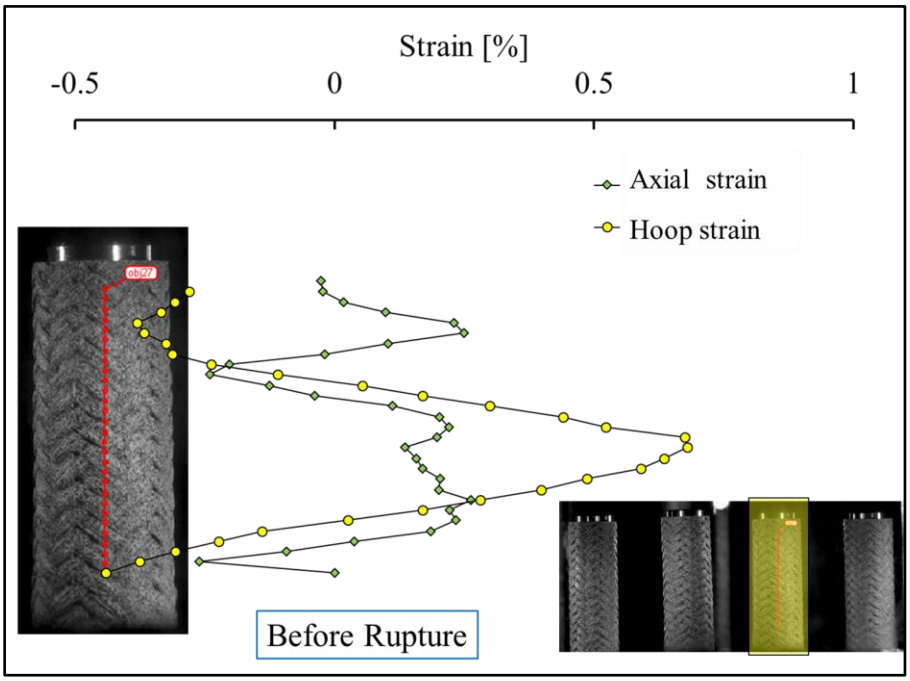

Figure 10 The distribution of the hoop and axial strain along the sample surface before the moment of rupture.

4.3 Discussion

SiC/SiC samples were subjected to the MBT using a DIC system that is capable of viewing the entire outer surface of the samples. Because a 360° view of the sample outer surface was captured by only one camera and an array of mirrors, the resolution of the strain measurement was lower than the resolution of measurements made by single-surface DIC systems. Therefore, the anisotropy in the strains caused by the yarn architecture was not determined. The strains calculated by the DIC objects involving multiple yarns reflected average strain values over the multiple yarns, which enables determination of the failure strains. The failure strains can be used as early data to validate the models implemented in computational tools for nuclear fuel cladding behavior.

The DIC system determined an upward movement of the sample, including vibrations, as a result of core-pin-induced pressurization at high speed. The upward movement of the sample and vibrations likely affect the strain measurement. If those effects exist, it is desirable to minimize them using either a new frame design or modifications to the DIC software.

We observed an increase in failure strain with increased pressurization rate, but that observation was based on a limited number of experiments. We are not yet reporting a specific conclusion or a mechanism relevant to the results because of the limited number of experiments, possible uncertainties caused by the strain determination, and frame/sample movement as a result of core-pin impact. Nevertheless, the preliminary results indicate some sources of potential uncertainties, including the uneven braided surface on the SiC/SiC samples and the fact that pinpointing “failure” with this kind of complex composite structure can be difficult.

One key metric of behavior during RIA for SiC/SiC cladding candidates is the definition of failure for SiC/SiC tubes. The SiC/SiC rupture is brittle with an extended load-carrying capacity, known as “pseudo-ductility, due to the SiC fiber architecture. The ultimate rupture is determined by the individual fiber strength, but the microcracking of the SiC matrix interconnected with the initial porosity of SiC/SiC

may lead to the release of the fission products. Thus the cooperation of the initial porosity with the matrix microcracking during RIA may lead to a loss of hermeticity of the cladding. Hence, the microcracking of the SiC matrix of SiC/SiC cladding calls into question the exact point of failure.

During a postulated RIA, the cladding is subjected to a biaxial strain state by isotropic expansion of the nuclear fuel during the PCMI phase or by the increasing internal gas pressure for the high-temperature phase [6]. Therefore, prototypic mechanical testing intended to evaluate cladding performance during RIA requires reproducing the strain state imposed during the transient. In this report, the strain biaxiality ratio was determined in the range of 0.42 to 0.9. The large variation in the strain biaxiality is likely caused by the upward movement of the sample and the frame. Sources of uncertainty include (1) possible vibrations that the DIC software is not completely capable of resolving on the sample surface and (2) the reduced resolution due to the use of mirrors and a single camera to capture a 360° view.

The strain-state evolution during MBT has not been previously addressed in the literature. Because cladding is expected to be under a biaxial strain state in RIA, it is important to understand the implications of strain state during MBT to appropriately inform development of computational models and possible failure limits for ATF cladding. The novel DIC system developed in FY 2017 provides new insights into the strain state during MBT.

5. SUMMARY AND FUTURE WORK

This report summarizes the research activities performed on the development of experiments to evaluate the response of fresh and irradiated candidate ATF cladding specimens for different RIA-like conditions relevant to PCMI. To achieve various RIA-like conditions, the MBT device was improved to produce different mechanical pulses by modifying the motion of the core pin. The calibration of the MBT instrument was accomplished by performing mechanical tests on unirradiated Gen-I FeCrAl alloy samples. The hoop strain was monitored using strain gauges attached on the sample surface in hoop direction.

Because of the uncertainty of the failure location on the sample surface, a DIC system composed of a single camera and an array of six mirrors was developed for the MBT instrument. The mirror arrangement enables a 360° observation of the sample's outer surface and thus enables determination of the exact failure location. SiC/SiC composite samples were tested using the DIC system at various pressurization rates of the driver tube (which correspond to the strain rate on the sample). The hoop strains for various loading conditions were determined for the SiC/SiC composites. The research plan of the separate-effects transient testing of ATF cladding candidates for FY 2018 will include further testing.

5.1 Aged FeCrAl Modified Burst Tube Testing

Irradiation studies of model FeCrAl alloys, which are candidates for ATF cladding, indicate that the dominant impact of the neutron radiation environment is the accelerated formation of Cr-rich α′ precipitates [24]. These precipitates form at high temperatures (300°C–400°C) as a result of the aging process, but their formation is accelerated under neutron irradiation. PCMI during RIA is not expected to be a possible failure mechanism for FeCrAl cladding, but it has not been conclusively shown using model FeCrAl alloys with Cr-rich α′ precipitates. MBT of as-manufactured Gen-I FeCrAl alloys was performed in FY 2016 and FY 2017 at Oak Ridge National Laboratory, but those alloys do not have representative mechanical properties of in-pile FeCrAl alloys, given that they have not been exposed to elevated temperatures and/or neutron irradiation. Because elevated temperatures in the absence of irradiation also produce α′ precipitates, FeCrAl samples will be aged in autoclaves, characterized, and tested using the MBT device to determine their response to strain-driven, high-strain-rate mechanical pulses that are

intended to mimic the dynamic behavior of RIA. Tests on the treated FeCrAl specimens will be used to determine changes in high-strain-rate failure behavior after precipitate formation and to provide key information about whether PCMI due to RIA is expected to be a failure mechanism for FeCrAl. This activity will also be used to determine whether an RIA failure of FeCrAl cladding is even possible. The L3 report will document the aging of the FeCrAl samples, characterization of the precipitates, and testing of the samples.

5.2 Informing In-pile Transient Reactor Test Design and Failure Limits using SiC/SiC Tests

High-strain-rate MBT has never been used to inform in-pile RIA test design, to develop failure limits based on strain/strain rate, or to support US Nuclear Regulatory Commission rulemaking. The objective of this activity is to take the data from the detailed SiC/SiC tests using DIC in FY 2017 and to use the data to develop a package of functional requirements for in-pile testing in the TREAT reactor. For example, the failure data will be used to determine the energy deposition that would produce a given failure strain and the combination of reactor kinetics parameters and reactivity insertion that would produce a given strain rate. The results will be used to determine the pulse characteristics of in-pile tests that would be expected to achieve cladding survival or to produce cladding failure. This activity is intended to demonstrate the usefulness of separate-effects test data in generating an envelope of test conditions for integral tests. The L3 will include an example envelope of failure criteria for SiC/SiC based on the MBT results and a set of corresponding RIA transients that would be expected to produce similar strain and strain rate behavior due to PCMI. Those conditions would be used to describe the energy deposition, fuel thermal expansion, and thermal-fluid conditions expected in an integral TREAT test. This activity will include an investigation of the appropriate stress state in the cladding and scoping investigations of potential modifications to the MBT. Initial tests using DIC also indicate that the MBT produces a stress state only in the hoop direction, whereas a somewhat biaxial stress state is expected in an actual RIA. Specifically, during an RIA event with postulated PCMI, the hoop stress is expected to be the maximum component of the stress in the cladding, but an axial tensile stress is also expected.

5.3 Other Activities

Other activities as part of the scope will include the continued development of the capability to conduct MBTs at elevated-temperature, improvements in the MBT stress biaxiality so that it is more prototypical of an RIA, and continued DIC development.

6. REFERENCES

[1] H. of Representatives, 122th Congress 1st Session Report 112-331, 2012, (2011) 90.
[2] S.J. Zinkle, K.A. Terrani, J.C. Gehin, L.J. Ott, L.L. Snead, Accident tolerant fuels for LWRs: A perspective, J. Nucl. Mater. 448 (2014) 374–379. doi:10.1016/j.jnucmat.2013.12.005.
[3] K.A. Terrani, S.J. Zinkle, L.L. Snead, Advanced oxidation-resistant iron-based alloys for LWR fuel cladding, J. Nucl. Mater. 448 (2014) 420–435. doi:10.1016/j.jnucmat.2013.06.041.
[4] B.A. Pint, K.A. Terrani, M.P. Brady, T. Cheng, J.R. Keiser, High temperature oxidation of fuel cladding candidate materials in steam–hydrogen environments, J. Nucl. Mater. 440 (2013) 420–427. doi:10.1016/j.jnucmat.2013.05.047.
[5] N.R. Brown, M. Todosow, A. Cuadra, Screening of advanced cladding materials and UN–U3Si5 fuel, J. Nucl. Mater. 462 (2015) 26–42. doi:10.1016/j.jnucmat.2015.03.016.
[6] J. Desquines, D.A. Koss, A.T. Motta, B. Cazalis, M. Petit, The issue of stress state during mechanical tests to assess cladding performance during a reactivity-initiated accident (RIA), J. Nucl. Mater. 412 (2011) 250–267. http://www.sciencedirect.com/science/article/pii/S002231151100273X.
[7] U.S. NRC, NRC: 10 CFR Appendix A to Part 50—General Design Criteria for Nuclear Power Plants, n.d. https://www.nrc.gov/reading-rm/doc-collections/cfr/part050/part050-appa.html.
[8] N.R. Brown, A.J. Wysocki, K.A. Terrani, K. Xu, D.M. Wachs, The potential impact of enhanced accident tolerant cladding materials on reactivity initiated accidents in light water reactors, Ann. Nucl. Energy. (2016). doi:http://dx.doi.org/10.1016/j.anucene.2016.09.033.
[9] M. Liu, N.R. Brown, K.A. Terrani, A.F. Ali, D.M. Blandford, E. D., Wachs, Potential impact of accident tolerant fuel cladding critical heat flux characteristics on the high temperature phase of reactivity initiated accidents, Ann. Nucl. Energy. (2017).
[10] K. Yueh, J. Karlsson, J. Stjärnsäter, D. Schrire, G. Ledergerber, C. Munoz-Reja, L. Hallstadius, Fuel cladding behavior under rapid loading conditions, J. Nucl. Mater. 469 (2016) 177–186. doi:10.1016/j.jnucmat.2015.11.032.
[11] M.N. Cinbiz, N.R. Brown, K.A. Terrani, R.R. Lowden, D. Erdman, A pulse-controlled modified-burst test instrument for accident-tolerant fuel cladding, Ann. Nucl. Energy. 109 (2017) 396–404. doi:10.1016/j.anucene.2017.05.058.
[12] B.N. Nobrega, J.S. King, G.S. Was, S.B. Wisner, Improvements in the design and analysis of the segmented expanding mandrel test, J. Nucl. Mater. 131 (1985) 99–104. doi:10.1016/0022-3115(85)90448-9.
[13] K.-F. Nilsson, O. Martin, C. Chenel-Ramos, J. Mendes, The segmented expanding cone-mandrel test revisited as material characterization and component test for fuel claddings, Nucl. Eng. Des. 241 (2011) 445–458. doi:10.1016/j.nucengdes.2010.10.026.
[14] H. Jiang, J.-A.J. Wang, Methodology for mechanical property testing of fuel cladding using an expanding plug wedge test, J. Nucl. Mater. 446 (2014) 27–37. doi:10.1016/j.jnucmat.2013.11.026.
[15] T. Shinozaki, Y. Udagawa, T. Mihara, T. Sugiyama, M. Amaya, Improved-EDC tests on the Zircaloy-4 cladding tube with an outer surface pre-crack, J. Nucl. Sci. Technol. 53 (2016) 1426–1434. doi:10.1080/00223131.2015.1123658.
[16] V. Grigoriev, R. Jakobsson, D. Schrire, Further development of mechanical test simulate RIA in irradiated cladding, in: 24th NSRR Tech. Rev. Meet. (JAERI-Conf 2001-010), JAERI, Ibaraki-ken, Japan, 2001: pp. 139–149.
[17] M.N. Cinbiz, N.R. Brown, R.R. Lowden, D. Erdman, K.A. Terrani, Issue Report Documenting Simulated PCI Testing, Oak Ridge, TN, 2016.
[18] Montgomery, R., R. Yang, Topical report on reactivity-initiated accident: Bases for RIA fuel and core coolability criteria, 2002.
[19] D.D. Imholte, F. Aydogan, Comparison of nuclear pulse reactor facilities with reactivity-initiated-accident testing capability, Prog. Nucl. Energy. 91 (2016) 310–324. doi:10.1016/j.pnucene.2016.05.012.

[20] Massih, A. R., L.O. Jernkvist, Nuclear Fuel Behaviour under Reactivity-initiated Accident (RIA) Condition: State-of-the-art Report, 2010.
[21] D. Crawford, R. Swanson, A. Wright, R. Holtz, RIA Testing Capability of the Transient Reactor Test Facility, in: Fuel Cycle Options Light Water React. Heavy Water React., 1999: p. 99.
[22] Y. Yamamoto, B.A. Pint, K.A. Terrani, K.G. Field, Y. Yang, L.L. Snead, Development and property evaluation of nuclear grade wrought FeCrAl fuel cladding for light water reactors, J. Nucl. Mater. 467 (2015) 703–716. doi:10.1016/j.jnucmat.2015.10.019.
[23] Y. Yamamoto, Z. Sun, B.A. Pint, K.A. Terrani, Optimized Gen-II FeCrAl cladding production in large quantity for campaign testing, Oak Ridge, 2016. http://info.ornl.gov/sites/publications/files/Pub67815.pdf.
[24] K.G. Field, S.A. Briggs, P. Edmondson, X. Hu, K.C. Littrell, R. Howard, C.M. Parish, Y. Yamamoto, Evaluation of the Effect of Composition on Radiation Hardening and Embrittlement in Model FeCrAl Alloys, Oak Ridge, 2015.